Ann. Geophys., 44, 689–696, 2026
https://doi.org/10.5194/angeo-44-689-2026

Annales Geophysicae
Open Access

Harmonic content of Ap index

Marek Vandas[1], **Evgeny Romashets**[2], **Tasmina Imam**[2], **Tanvir Hasan**[2], **Pranab Majumder**[2], **and Sanjay Karki**[2]

[1]Astronomical Institute of the Czech Academy of Sciences, Prague, Czech Republic
[2]Department of Physics, Lamar University, Beaumont, Texas, USA

Correspondence: Evgeny Romashets (eromashets@lamar.edu)

Received: 20 September 2025 – Discussion started: 14 October 2025
Revised: 10 June 2026 – Accepted: 13 July 2026 – Published: 28 July 2026

Abstract. Fourier spectral analysis is applied to the planetary geomagnetic index Ap for the February 2001, 2003, and 2017 time intervals. We investigate how Fourier coefficients change in time with respect to geomagnetic activity. A detailed analysis of the 13–14 February 2001 substorm revealed that higher harmonics were suppressed during the event, contrary to what was expected.

1 Introduction

Geomagnetic indices Kp and Ap, introduced by Bartels (1949, 1957), provide a widely used measure of magnetospheric convection strength (e.g., Thomsen, 2004; Rowland and Wygant, 1998; Wang et al., 2025). Large-scale magnetospheric convection is driven by day- and night-side magnetic reconnection (Siscoe and Huang, 1985; Cowley and Lockwood, 1992; Dai et al., 2024; Zhu et al., 2024, 2025, etc.) and penetrates deep into the inner magnetosphere (e.g., Wygant et al., 1998; Dai et al., 2015; Thaller et al., 2015). Abe et al. (2023) compared the spectral content of geomagnetic indices and the Sunspot Number (SSN) during solar cycles 23 and 24. Zajtsev et al. (1993) and De Michelis et al. (2014) considered Fourier spectra of the geomagnetic field. Rangarajan and Lyemori (1997) analyzed data on the Kp and Ap indices from 1932 to 1960 and found that the relative frequencies of Kp with different magnitudes show consistent seasonal and solar-cycle dependencies. de Gonzalez et al. (1993) investigated a different set of Ap data using the power spectrum technique. The monthly Ap power spectrum reveals a period around 4 years, associated with a double peak structure in geomagnetic activity. Daily Ap spectrum peaks are interpreted as harmonics of a 6-month period, and others as linked to solar rotation periodicity, suggesting the juxtaposition of two Fourier sequences.

Another geomagnetic index, Dst, better describes the intensity and position of the ring current, which influences the H-component of the Earth's surface geomagnetic field. Le Mouel et al. (2019) identified several significant spectral components in Dst data using singular spectrum analysis, namely a prominent 6-month component, along with 47, 10.6, 1, 22, 11 and 5.5 year components. Rigozo et al. (2006) applied spectral analysis to the annual and monthly average series of Ap from 1868 to 2001. Riabova and Spivak (2018) used a similar approach to the data from the Mikhnevo Geophysical Observatory in 2009–2015. Riabova (2018) developed a wavelet model for analyzing geomagnetic field variations, which demonstrated effectiveness in detecting sudden commencements.

The study of Pai and Sarabhai (1964) examines periodic fluctuations in the Earth's magnetic field during magnetic storms using data from 1958. Autocorrelation analysis reveals a common 40 min period for fluctuations, primarily during geomagnetic storms. Cliver et al. (1996) proposed that changes in geomagnetic activity associated with alternating sunspot maxima are primarily driven by solar variations, including stronger 27 d recurrent solar wind streams.

Zajtsev et al. (1993) applied fast Fourier transform (FFT) (Cooley et al., 1969) of the magnetic field components measured by a particular magnetic observatory. They reported that some patterns could be recognized in the contour plots of the Fourier coefficients versus time for different phases of substorms.

We present the Fourier decomposition of the Ap index for the February 2001, 2003, and 2017 periods. We focus on changes in spectral content during increased geomagnetic activity. The next section describes the method used in this

Published by Copernicus Publications on behalf of the European Geosciences Union.

work. The results are presented in Sect. 3. Finally, a discussion and conclusions are given in Sect. 4.

2 Method

We consider the Ap index as a function of time that can be decomposed into the Fourier sum with the fundamental angular frequency $\omega = \frac{2\pi}{T}$, where the period is $T = 27$ d. The index is calculated per three hour time interval, that is, the data in $K = 27 \cdot 8 = 216$ intervals are used. Consider the function $\mathrm{Ap}(t)$ in the time interval $\left[\frac{l}{K}T,\ \frac{l}{K}T + T\right]$ where $l \geq 0$ is an integer, and introduce a function $\mathrm{Ap}_l(t')$ defined for $t' \in \left[-\frac{T}{2}, \frac{T}{2}\right]$ by

$$\mathrm{Ap}_l(t') = \mathrm{Ap}\left[t' + \left(\frac{l}{K} + \frac{1}{2}\right) T\right]. \tag{1}$$

The function $\mathrm{Ap}_l(t')$ is then approximated by a finite Fourier series

$$\begin{aligned} \mathrm{Ap}_l(t') &= a_{0l} + \sum_{n=1}^{N} \left(a_{nl} \cos n\omega t' + b_{nl} \sin n\omega t'\right) \\ &= c_{0l} \cos\phi_0 + \sum_{n=1}^{N} c_{nl} \cos n(-\phi_{nl}/n + \omega t'). \end{aligned} \tag{2}$$

Introducing discrete values $t'_{lk} = t_k - \left(\frac{l}{K} + \frac{1}{2}\right) T$, $\mathrm{Ap}(t_k) = \mathrm{Ap}_k$, $t_k = \frac{k}{K} T$, the coefficients a_{nl}, b_{nl}, c_{nl}, and phases ϕ_{nl} are calculated as follows:

$$a_{0l} = \frac{1}{K} \sum_{k=l}^{l+K} \mathrm{Ap}_k - \frac{1}{2K} \left(\mathrm{Ap}_l + \mathrm{Ap}_{l+K}\right), \tag{3}$$

$$\begin{aligned} a_{nl} = \sum_{k=l}^{l+K-1} \Bigg[& \frac{K}{2n^2\pi^2} (\mathrm{Ap}_{k+1} - \mathrm{Ap}_k) (\cos n\omega t'_{l,k+1} - \cos n\omega t'_{l,k}) \\ & + \frac{1}{n\pi} (\mathrm{Ap}_{k+1} \sin n\omega t'_{l,k+1} - \mathrm{Ap}_k \sin n\omega t'_{l,k}) \Bigg],\ n > 0, \end{aligned} \tag{4}$$

$$\begin{aligned} b_{nl} = \sum_{k=l}^{l+K-1} \Bigg[& \frac{K}{2n^2\pi^2} (\mathrm{Ap}_{k+1} - \mathrm{Ap}_k) (\sin n\omega t'_{l,k+1} - \sin n\omega t'_{l,k}) \\ & - \frac{1}{n\pi} (\mathrm{Ap}_{k+1} \cos n\omega t'_{l,k+1} - \mathrm{Ap}_k \cos n\omega t'_{l,k}) \Bigg],\ n > 0, \end{aligned} \tag{5}$$

$$c_{0l} = |a_{0l}|, \tag{6}$$

$$c_{nl} = \sqrt{a_{nl}^2 + b_{nl}^2},\ n > 0 \tag{7}$$

$$\phi_{0l} = 0,\ a_{0l} > 0 \tag{8}$$

$$\phi_{0l} = \pi,\ a_{0l} < 0 \tag{9}$$

$$\phi_{nl} = \arctan(a_{nl}, b_{nl}),\ n > 0, \tag{10}$$

where arctan of two arguments returns values in the full range $[0, 2\pi)$ and reduces to ordinary arctan $\frac{b_{nl}}{a_{nl}}$ for $a_{nl} > 0$, $b_{nl} \geq 0$. Here, c_{nl} are the amplitudes of the particular harmonics and ϕ_{nl} are their phases, while a_{nl} and b_{nl} are Fourier coefficients. The coefficient a_{0l} is calculated via integration

$$a_{0l} = \frac{1}{T} \int_{-T/2}^{T/2} \mathrm{Ap}_l(t')\, \mathrm{d}t' \tag{11}$$

Because the function Ap_l defined earlier is known only at times separated by three hours, we use linear interpolation, and the integration (11) becomes the sum of 216 areas of the corresponding trapezoids in (3). The summation is over k from $k = l$ which corresponds to $t' = -T/2$, to $k = l + K$ which corresponds to $t' = T/2$. The area of the trapezoid determined by two points Ap_k and Ap_{k+1} is $(\mathrm{Ap}_k + \mathrm{Ap}_{k+1})T/(2K)$. All Ap_k appear twice, except the very first and the last in the sum, which appear only once.

Similarly, the coefficients a_{nl} and b_{nl} in (4) and (5) are calculated by integrations

$$a_{nl} = \frac{2}{T} \int_{-T/2}^{T/2} \mathrm{Ap}_l(t') \cos n\omega t'\, \mathrm{d}t', \tag{12}$$

$$b_{nl} = \frac{2}{T} \int_{-T/2}^{T/2} \mathrm{Ap}_l(t') \sin n\omega t'\, \mathrm{d}t', \tag{13}$$

which again results in sums with respect to k. The difference is that now each element of the sums is not simply the trapezoid area but the actual integral of the linearly interpolated $\mathrm{Ap}_l(t')$ multiplied by $\cos n\omega t'$ or $\sin n\omega t'$ in a time interval of three hours. The interpolation is given by

$$\mathrm{Ap}_l(t') = \mathrm{Ap}_k + \frac{\mathrm{Ap}_{k+1} - \mathrm{Ap}_k}{T} \left(t' + \frac{T}{2}\right),\quad t' \in \left[-\frac{T}{2}, \frac{T}{2}\right]. \tag{14}$$

Both c_{nl} and ϕ_{nl} depend on two indexes, in frequency and in time. The step along l corresponds to three hours in time, while a step along n means an increase in frequency by ω. In other words, all coefficients and phases are calculated in (3)–(5) for every three-hour interval. We use Ap data of 27 days. N was set equal to $K/2 = 108$. For any particular time, t, which is determined by $k = t/3$, time in hours, k in three-hour intervals from the beginning of the year, the allowed values of l are in the range $[k - 215, k - 1]$, and the allowed starting time of t is in the range $[3k - 645, 3k - 3]$. On the other hand, for a given l, there is only one set of coefficients a_{nl} and b_{nl}.

3 Results

The time profiles of the Ap index for the Februaries 2001, 2003 and 2017 are shown in Fig. 1. The intervals contain relatively long quiet periods, with Ap < 20 nT, and strong disturbances with Ap up to 60 nT. The graphs are supplemented by profiles of the Dst index.

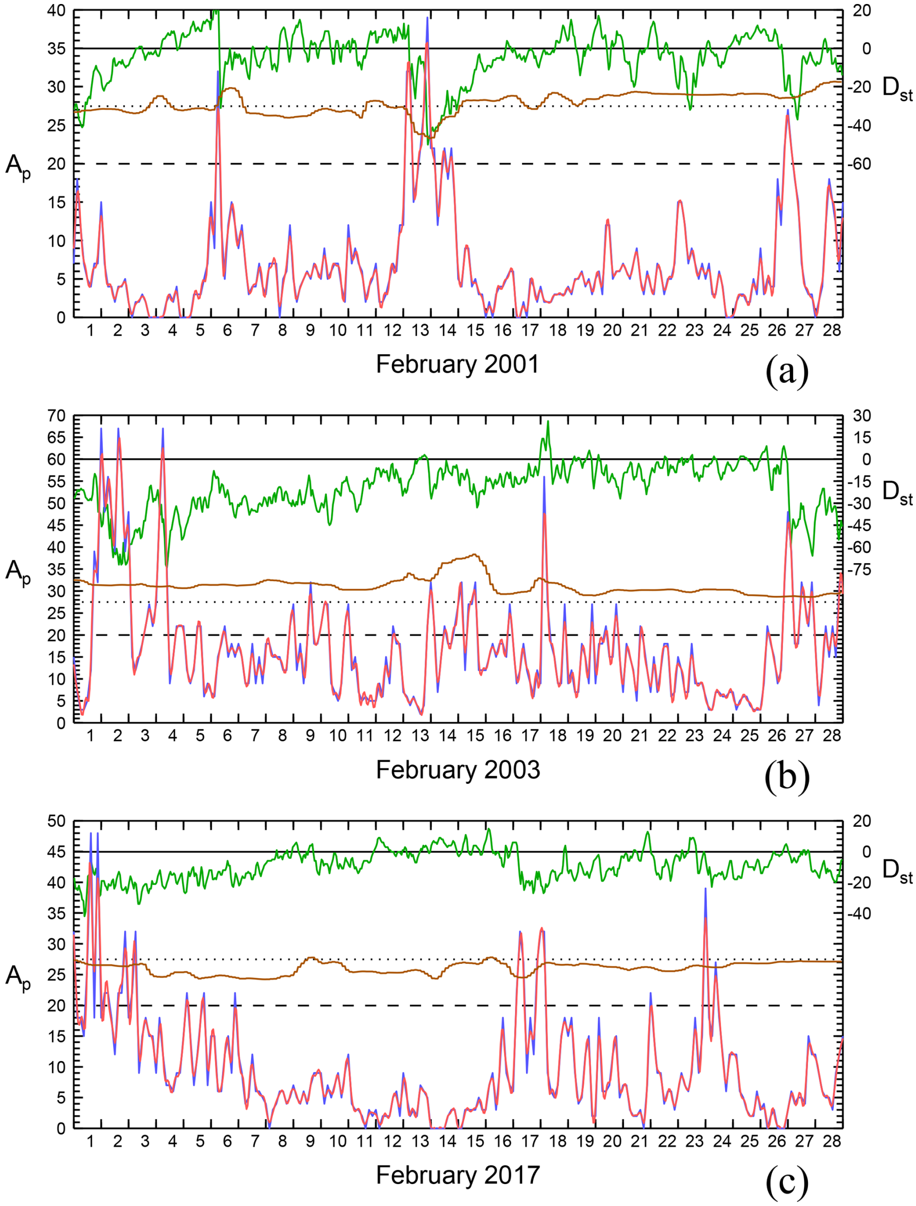

Figure 1. Ap time profiles for our three time periods. The blue lines represent the original data, but they are mostly obscured by the red lines showing the reconstructed Ap. The dashed horizontal lines indicate Ap = 20 nT. Dst index is drawn by the green lines in the top part of the panels, with the scales on the right hand side and the horizontal solid lines indicating Dst = 0 nT. The brown lines in the middle part of the panels are explained in the text.

The Fourier harmonics with $N = 108$ work very well for February 2001, as one can see from Fig. 1a. The original data and the reconstructed Ap are practically indistinguishable for most of the month. The reconstruction is done in the following way. For a given time t, the closest t_k is found that $t \leq t_k$. The interval $\left[\frac{l}{K}T, \frac{l}{K}T + T\right]$, for which the coefficients a_{nl} and b_{nl} are calculated, is centered at t_k. This specifies the value of l: $l = k - \frac{K}{2}$. Then a_{nl} and b_{nl} are determined from Eqs. (3)–(5) and the reconstructed Ap(t) from Eqs. (1)–(2).

The month of February 2001 was relatively quiet, with $\mathrm{Ap}_{\mathrm{max}} = 40$ nT, without abrupt peaks. On the other hand, February 2003 was a very disturbed month, with $\mathrm{Ap}_{\mathrm{max}} = 70$ nT, and rapid transitions from nearly smooth behavior changed to abrupt jumps. The reconstruction follows the data very well, but some minor deviations can be seen from time to time. February 2017 was a relatively quiet month. The reconstructed and real data are very close to each other.

The two-dimensional functions c_{nl} and ϕ_{nl} can be represented as contour plots. The contour plots of c_{nl} for our three

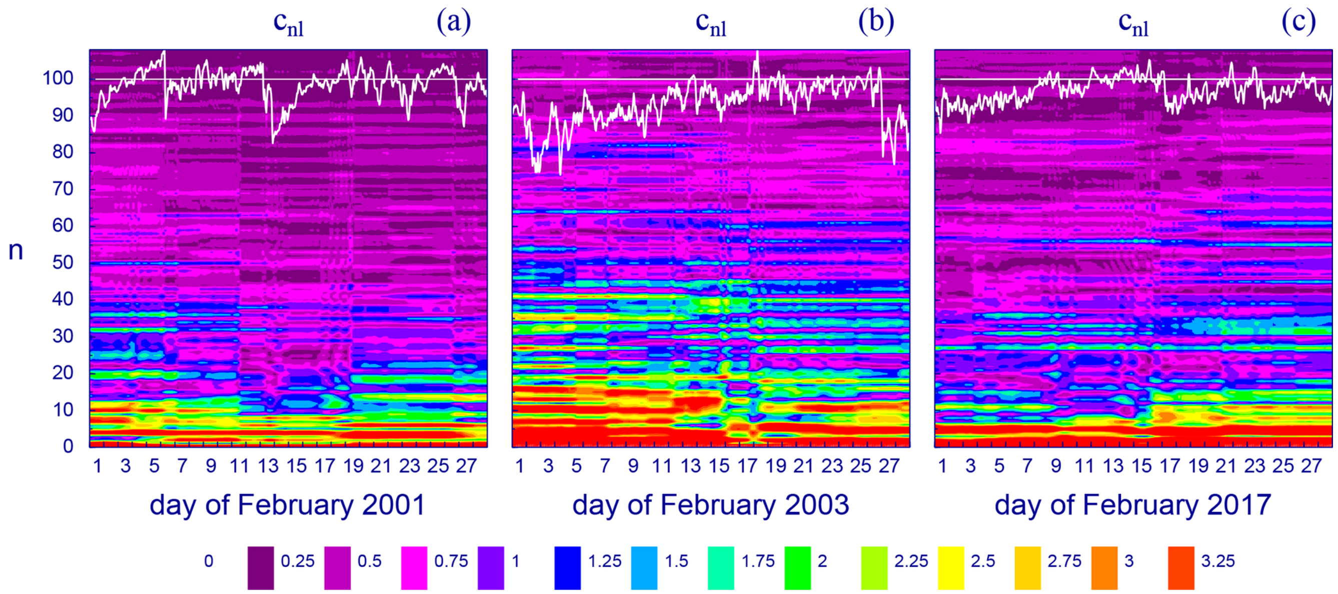

Figure 2. Contour plots of c_{nl} for our three periods under consideration. They are supplemented by Dst profiles in the top parts as the white lines. The Dst values are in arbitrary units but their scales are identical and the white horizontal lines indicate a zero value.

periods are shown in Fig. 2. In the contour plots, the horizontal axis represents time, and the vertical axis represents n. The angular frequency ω_n and n are related as $\omega_n = n\omega$. For example, $n = 10$ corresponds to frequency 103 µHz. The l is associated with time as has been described above. It can be seen that maximum intensities occur at low frequencies. As frequency increases, the value of c_{nl} decreases. Fig. 2 shows the pronounced structure at the lower frequency components, probably associated with atmospheric tides (Chen et al., 2024).

Raw magnetic data typically show atmospheric tides at diurnal and semi-diurnal periods, corresponding to $n = 27$ and $n = 54$. The effect is especially pronounced in February 2017 and 2003; there are clear lines in the lower frequencies. February 2001 was more active, and the atmospheric tide effects were weaker. This means that geomagnetic activity covers the magnetic signatures of atmospheric tides and also planetary waves (at lower n), which are visible in the Ap time series. The disappearance of tidal signals in Ap indicates geomagnetic activity.

The contour plots of the modified and normalized phase ϕ_{nl} are demonstrated in Fig. 3. Eqs. (8)–(10) yield values between 0 and 360°. The ϕ_{nl} was modified to make it continuous (by adding or subtracting a multiple of 360°). Consequently, ϕ_{nl} was normalized by division by n (it appears in this form in Eq. 2). The contour plots show that modified and normalized ϕ_{nl} decreases nearly monotonically over time. And Fig. 4 shows that this decrease is nearly linear. Deviations from the linear trend are observed during periods of increased geomagnetic activity. For example, in February 2017, a relatively quiet period, most normalized and modified ϕ_{nl} are straight lines. Figure 5 displays the root mean square (RMS) of modified and normalized ϕ_{nl} for selected frequency bands. During the solar maximum (2001, 2003), the band 1–19 hits 90° in the beginning, whereas during the relatively quiet period (2017) it hits 0° in the beginning. The other bands of the phase angles show similar temporal profiles, hitting nearly 0° in the beginning.

The right part of Eq. (2) suggests a complex form of Ap,

$$\mathrm{Ap}^c(t) = \sum_{n=0}^{N} c_{nl} \mathrm{e}^{i\left\{n\omega\left[t-\left(\frac{l}{K}+\frac{1}{2}\right)T\right]-\phi_{nl}\right\}}. \tag{15}$$

The real part of Ap^c is equal to Ap. The hodographs (Fig. 6) show the behavior of the complex Ap^c. A hodograph represents the path traced out by the tip of a vector (here a complex number) as it moves over time. No physical conclusions are drawn from the imaginary part. The hodographs reveal clear differences in geomagnetic activity across solar cycle phases: February 2001 (solar maximum) shows large, widely spread loops indicating intense storm activity, while February 2003 exhibits more compact trajectories with moderate disturbances. By contrast, February 2017 (solar minimum) shows fewer and tighter loops, reflecting quieter geomagnetic conditions.

Our intention was to search for changes in the c_{nl} coefficients (or phases) with geomagnetic activity. We anticipated that the higher-frequency coefficients intensify during disturbed periods. However, we do not see any distinct behavior of the coefficients with respect to Dst in Fig. 2. Therefore, we calculate the ratio of RMSs of the Fourier coefficients c_{nl} within two harmonic bands, namely RMS for $n = 15$–20 over RMS for $n = 5$–10, for every selected l. The ratio (with l converted to time) is shown as brown lines in Fig. 1. Here, the

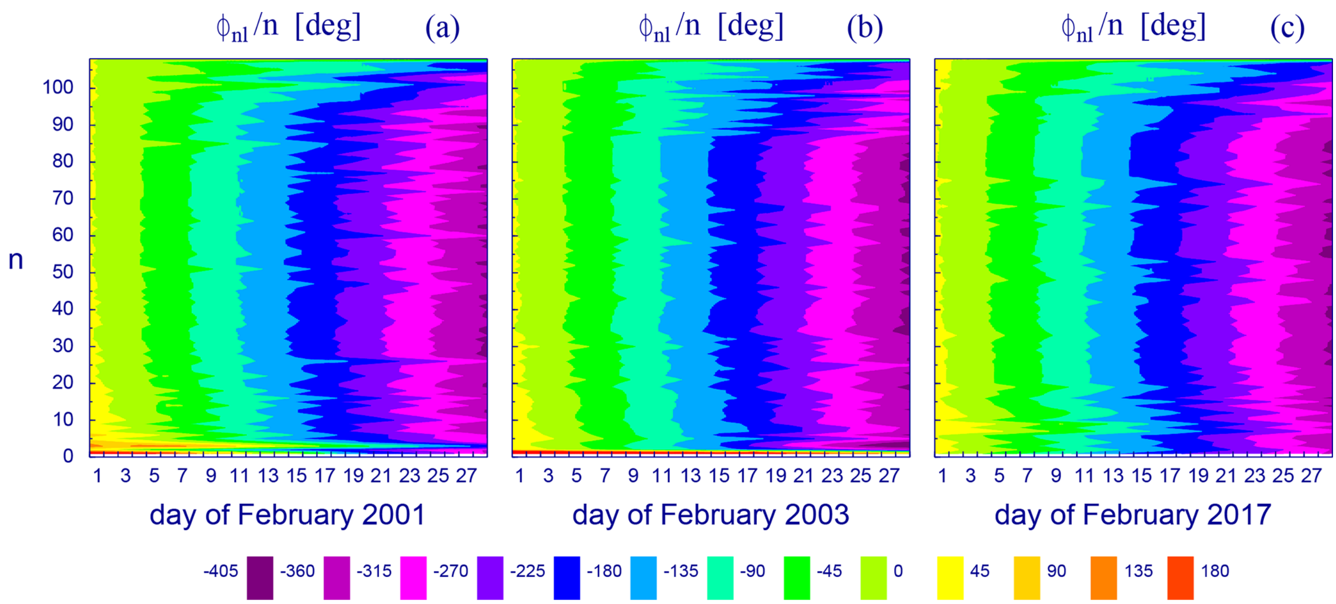

Figure 3. Contour plots of modified and normalized ϕ_{nl}.

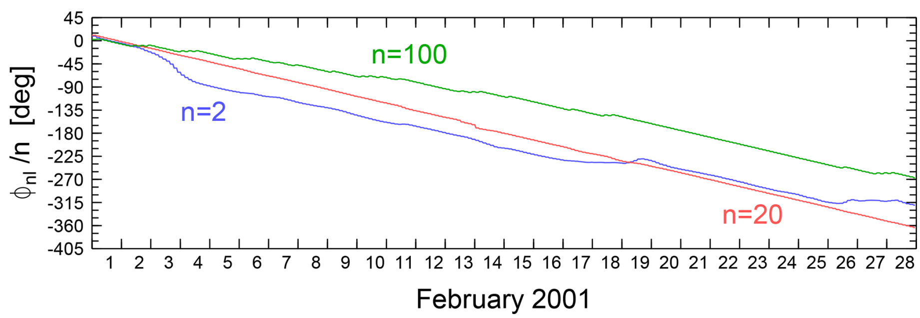

Figure 4. Profiles of modified and normalized ϕ_{nl} for three n in February 2001.

dashed and dotted horizontal lines indicate 0 and 0.5 values of this RMS ratio, respectively.

Similarly to Fig. 2, we do not see any one to one correspondence between the RMS ratio and geomagnetic activity in Fig. 1. However, one event drew our attention, namely a distinct substorm during 13–14 February 2001, in panel (a). A Dst decrease is followed by a recovery, the Ap values are greater than 20 nT. The event coincides with a distinct decrease in the RMS ratio, which means a suppression of higher frequencies, which was unexpected for us, because we anticipated an opposite effect, as has been mentioned above.

4 Discussion and conclusions

Fourier analysis of the linearly interpolated Ap index is performed for three monthly periods in 2001, 2003, and 2017. The coefficients near $\cos n\omega t$ and $\sin n\omega t$ in a Fourier series have been found. The Fourier reconstruction of Ap works well. One can see that the reconstructed Ap is in good agreement with the original data. The Fourier sum usually reconstructs functions better than the Fourier transform. In addition, one can add an imaginary counterpart, and thus hodographs can be plotted. The hodograph of February 2017 is uniformly spread over the complex surface, while those of 2001 and 2003 reveal a tendency for concentrations in a region close to the origin. This could be general properties of quiet and disturbed periods.

The Fourier coefficient magnitudes and phases change smoothly with time, while the index Ap is not very smooth. Our idea was that abrupt changes in the Ap index could be predicted based on analysis of variations in Fourier coefficients before abrupt changes occur. However, the presented analysis did not support it.

We noticed that during the 13–14 February 2001 substorm, intensity of higher frequencies decreases with respect to lower frequencies, which is an unusual and unexpected effect. Whether it is a general effect, or if it only holds for some class of substorms, or it is a mere coincidence, it deserves a future analysis. If it is the case for most geomagnetic storms,

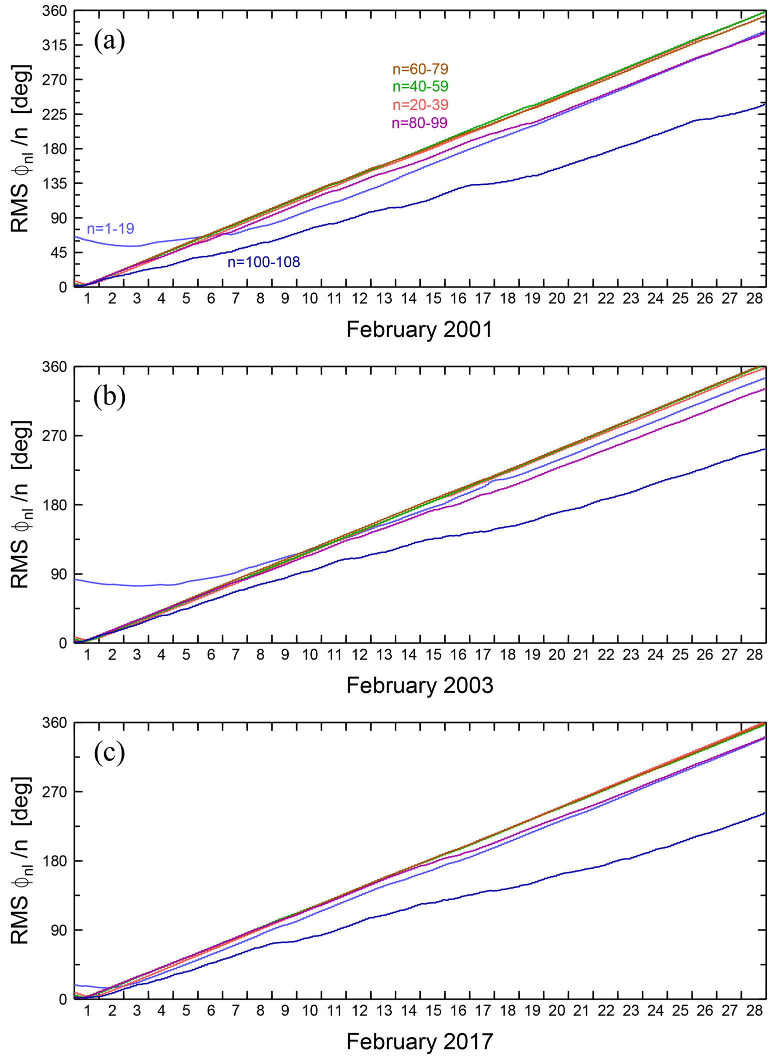

Figure 5. Profiles of RMS of modified and normalized ϕ_{nl} for six bands of n, distinguished by colors. Color-coding of parts **(b)** and **(c)** is the same as of **(a)**.

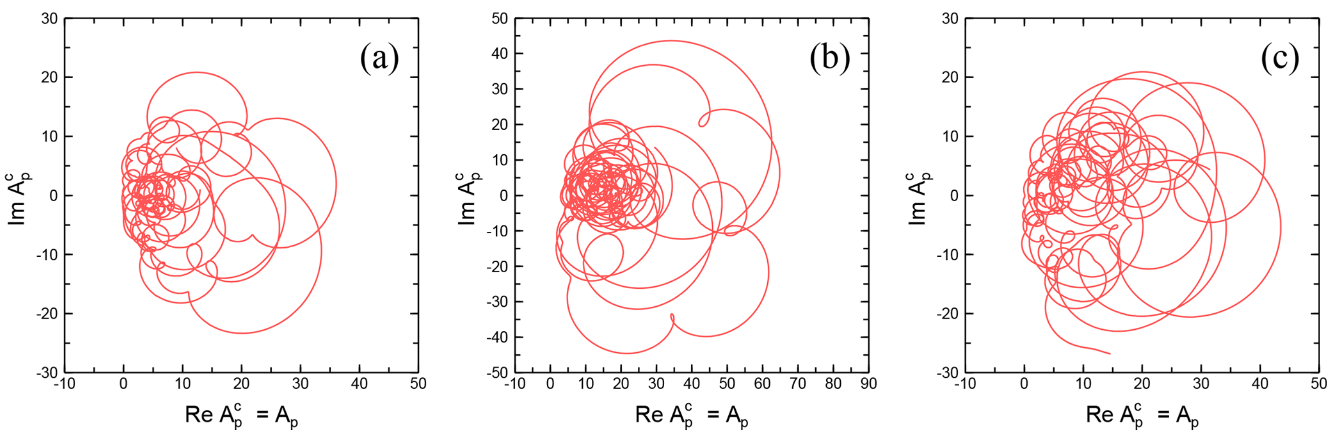

Figure 6. Hodographs of the complex Ap^c.

then there is no solar effect on the auroral index Ap and it is mainly determined by processes intrinsic to the magnetosphere.

Data availability. Data on Ap were taken from Geomagnetic Observatory Niemegk, GFZ German Research Centre for Geosciences, Potsdam, Germany (Matzka et al., 2021, ftp://ftp.gfz-potsdam.de/pub/home/obs/Kp_ap_Ap_SN_F107/, last access: 19 March 2024). Data on Dst were provided by World Data Center at Kyoto University (https://wdc.kugi.kyoto-u.ac.jp/dst_final/, last access: 9 March 2026).

Author contributions. E.R. suggested the method for harmonic analysis of Ap index, M.V. derived the formulas, performed calculations of the coefficients, and made all figures. T.I. developed Python codes. T.H. studied literature and developed codes. P.M. performed calculations. S.K. made a formal analysis. All authors wrote the text and made editing.

Competing interests. The contact author has declared that none of the authors has any competing interests.

Disclaimer. Publisher's note: Copernicus Publications remains neutral with regard to jurisdictional claims made in the text, published maps, institutional affiliations, or any other geographical representation in this paper. The authors bear the ultimate responsibility for providing appropriate place names. Views expressed in the text are those of the authors and do not necessarily reflect the views of the publisher.

Financial support. This research has been supported by the NSF grant 2230363. M. V. was supported by the AV ČR grant RVO:67985815.

Review statement. This paper was edited by Nour Dahmen and reviewed by three anonymous referees.

References

Abe, O. E., Fakomiti, M. O., Igboama, W. N., Akinola, O. O., Ogunmodimu, O., and Migoya-Orue, Y. O.: Statistical analysis of the occurrence rate of geomagnetic storms during solar cycles 20–24, Adv. Space Res., 71, 2240–2251, 2023.

Bartels, J.: The standardized index, Ks, and the planetary index, IATME Bull., 12b, 97–120, 1949.

Bartels, J.: The geomagnetic measures for the time-variations of solar corpuscular radiation, described for use in correlation studies in other geophysical fields, Ann. Intern. Geophys., 4, 227–236, 1957.

Chen, S. S., Yamazaki, Y., Denardini, C. M., Resende, L. C. A., Chagas, R. A. J., and Stolle, C.: Tidal composition analysis of global Sq current system, J. Geophys. Res., 129, e2023JA032382, https://doi.org/10.1029/2023JA032382, 2024.

Cliver, E. W., Boriakoff, V., and Bounar, K. H.: The 22-year cycle of geomagnetic and solar wind activity, J. Geophys. Res.-Space, 101, 27091–27109, 1996.

Cooley, J. W., Lewis, P. A., and Welch, P. D.: The fast Fourier transform and its applications, IEEE T. Educ., 12, 27–34, 1969.

Cowley, S. W. H. and Lockwood, M.: Excitation and decay of solar wind-driven flows in the magnetosphere-ionosphere system, Ann. Geophys., 10, 103–115, 1992.

Dai, L., Wang, C., Duan, S., He, Z., Wygant, J. R., Cattell, C. A., Tao, X., Su, Z., Kletzing, C., Baker, D. N., Li, X., Malaspina, D., Blake, J. B., Fennell, J., Claudepierre, S., Turner, D. L., Reeves, G. D., Funsten, H. O., Spence, H. E., Angelopoulos, V., Fruehauff, D., Chen, L., Thaller, S., Breneman, A., and Tang, X.: Near-Earth injection of MeV electrons associated with intense dipolarization electric fields: Van Allen Probes observations, Geophys. Res. Lett., 42, 6170–6179, https://doi.org/10.1002/2015GL064955, 2015.

Dai, L., Zhu, M., Ren, Y., Gonzalez, W., Wang, C., Sibeck, D., Samsonov, A., Escoubet, P., Tang, B., Zhang, J., and Branduardi-Raymont, G.: Global-scale magnetosphere convection driven by dayside magnetic reconnection, Nat. Commun., 15, 639, https://doi.org/10.1038/s41467-024-44992-y, 2024.

de Gonzalez, A. L., Gonzalez, W. D., Dutra, S. L., and Tsurutani, B. T.: Periodic variation in the geomagnetic activity: A study based on the Ap index, J. Geophys. Res.-Space, 98, 9215–9231, 1993.

De Michelis, P., Consolini, G., and Tozzi, R.: On the multi-scale nature of large geomagnetic storms: an empirical mode decomposition analysis, Nonlin. Processes Geophys., 19, 667–673, https://doi.org/10.5194/npg-19-667-2012, 2012.

Le Mouel, J. L., Lopes, F., and Courtillot, V.: Singular spectral analysis of the aa and Dst geomagnetic indices, J. Geophys. Res.-Space, 124, 6403–6417, 2019.

Matzka, J., Stolle, C., Yamazaki, Y., Bronkalla, O., and Morschhauser, A.: The geomagnetic Kp index and derived indices of geomagnetic activity, Spa. Weath., 19, e2020SW002641, https://doi.org/10.1029/2020SW002641, 2021.

Pai, G. L. and Sarabhai, V. A.: Periodic fluctuations in the geomagnetic field during magnetic storms, Planet. Space Sci., 12, 855–865, 1964.

Rangarajan, G. K. and Iyemori, T.: Time variations of geomagnetic activity indices Kp and Ap: an update, Ann. Geophys., 15, 1271–1290, https://doi.org/10.1007/s00585-997-1271-z, 1997.

Riabova, S.: Application of wavelet analysis to the analysis of geomagnetic field variations, J. Phys. Conf. Ser., 1141, 012146, https://doi.org/10.1088/1742-6596/1141/1/012146, 2018.

Riabova, S. A. and Spivak, A. A.: Variations in the K-index of geomagnetic activity in the Moscow Region, Izvestiya, Atmospheric and Oceanic Physics, 54, 705–710, 2018.

Rigozo, N. R., Echer, E., and Vieira, L. E. A.: Spectral analysis of sunspot number and geomagnetic indices (1868–2001), J. Atmos. Sol.-Terr. Phys., 68, 182–190, 2006.

Rowland, D. E. and Wygant, J. R.: Dependence of the large-scale, inner magnetospheric electric field on geomagnetic activity, J. Geophys. Res., 103, 14959–14964, https://doi.org/10.1029/97JA03524, 1998.

Siscoe, G. L. and Huang, T. S.: Polar cap inflation and deflation, J. Geophys. Res., 90, 543–547, https://doi.org/10.1029/JA090iA01p00543, 1985.

Thaller, S. A., Wygant, J. R., Dai, L., Breneman, A. W., Kersten, K., Cattell, C. A., Bonnell, J. W., Fennell, J. F., Gkioulidou, M., Kletzing, C. A., De Pascuale, S., Hospodarsky, G. B., and Bounds, S. R.: Van Allen Probes investigation of the large-scale duskward electric field and its role in ring current formation and plasmasphere erosion in the 1 June 2013 storm, J. Geophys. Res., 120, 4531–4543, https://doi.org/10.1002/2014JA020875, 2015.

Thomsen, M. F.: Why Kp is such a good measure of magnetospheric convection, Spa. Weath., 2, S11004, https://doi.org/10.1029/2004SW000089, 2004.

Wang, X., Dai, L., Wang, T., Ren, Y., Zhu, M., Yang, X., Wang, C., and Gonzalez, W.: Inner magnetospheric convection electric fields and corresponding geomagnetic indices during high-speed solar wind streams, Spa. Weath., 23, e2025SW004548, https://doi.org/10.1029/2025SW004548, 2025.

Wygant, J., Rowland, D., Singer, H. J., Temerin, M., Mozer, F., and Hudson, M. K.: Experimental evidence on the role of the large spatial scale electric field in creating the ring current, J. Geophys. Res., 103, 29527–29544, https://doi.org/10.1029/98JA01436, 1998.

Zajtsev, A. N., Ivanov, K. G., and Odintsov, V. I.: Structure and nature of spectra of the geomagnetic field in the case of very large magnetic storms (13–14 March 1989 and 8–9 Nov. 1991), Geomagnetism and Aeronomy, 33, 145–150, 1993.

Zhu, M., Dai, L., Wang, C., Gonzalez, W., Samsonov, A., Guo, X., Ren, Y., Tang, B., and Xu, Q.: The influence of ionospheric conductance on magnetospheric convection during the southward IMF, J. Geophys. Res., 129, e2024JA032607, https://doi.org/10.1029/2024JA032607, 2024.

Zhu, M., Dai, L., Ren, Y., Wang, X., Wang, T., Wang, K., and Wang, C.: Response of magnetospheric convection to the southward turning of the IMF in fast and slow solar wind streams, J. Geophys. Res., 130, e2025JA034529, https://doi.org/10.1029/2025JA034529, 2025.